NANOMATERIALS SCIENCE & ENGINEERING
Vol. 5, No. 1, pp. 17-24 (2023)

RESEARCH ARTICLE

https://doi.org/10.34624/nmse.v5i1.33484

Local piezoelectric properties of Di-Leucine dipeptides nanotubes

Igor Bdikin [1, 2, *]

[1]TEMA: Centre for Mechanical Technology and Automation, Department of Mechanical Engineering, University of Aveiro, Campus de Santiago, 3810-193 Aveiro, Portugal
[2]LASI—Intelligent Systems Associate Laboratory, Guimarães, Portugal
**Corresponding author, e-mail address: bdikin@ua.pt*

Received 13 September 2023; accepted 3 October 2023; published online 20 October 2023

ABSTRACT

Di-Leucine (LL) peptide nanotubes (PNTs) were grown. The local piezoelectric properties of LL PNTs were measured using atomic force microscopy. Using piezoresponse force microscopy the strong piezoelectric properties with d_{15} ~3.2 pm/V was found. The magnitude and distribution of the piezo response signal were analysed depending on the orientation of the tubes. Features of the charge distribution depending on the microstructure of LL PNTs were discovered by Kelvin Probe Force Microscopy.

1. INTRODUCTION

Di-peptides nanotubes (PNTs) have received much attention in the last decade because of their close relationship with life and the nanotube formation by various hydrophobic dipeptides and its structural properties were studied by many authors [1, 2]. These are materials absolutely corelated with biology (systhesis, physical and chemical properties, utilizations) and their have many potential applications in various broadening fields from medicine (as containers for medical, biosensors, etc [3-6]) to technology energy (harvesting), nanoelectronics [7], semiconducting nanostructures [8], colored surfaces [9], etc. Polypedide structure of PNTs is very close to polyt – DNR and RNR. So, PNTs are as well as genetic and tissue (protein) engineering. Tubular structures can be constructed with cyclic di-, tri-, tetra-, hexa-, octa-, and decapeptides with various amino acid sequences, enantiomers, and functionalized side chains and can be applied for antiviral and antibacterial drugs, drug delivery and gene delivery vectors, organic electronic devices, and ionic or molecular channels [10]. From another side known PNTs nanotubes structures have crystal structure what is possible to do analysis from material science point as conductor, semiconductor and possible to do controlled microstructure different blocks and elements for electronics [11], for example, dipeptides DiHpa, DiApp, and DiAph [12]. Hierarchical self-assembly Phe peptide blocks can form nano and micro-structures sized assemblies [13]. Self-assembly di-para-fluoro-Phe, di-pentafluoro-Phe, di-para-iodo-Phe, di-4-phenyl-Phe, di-para-nitro-Phe well-ordered nanostructures [14] and morphological twist in Phe-Phe dipeptide conjugates [15] were obtained. Self-assembly of Fc-coupled diphenylalanine (Phe-Phe, FF) and then used as supporting matrix for immobilization of glucose oxidase (GOx) were synthesized [16]. Self-organization Asp-Phe PNTs, Tyr-Ala (YA) and Asp-Phe [17], metal-mediated modification of spherical soft assemblies Phe–Phe dipeptide [18] are known. The peptide H-Phe(4-azido)- Phe(4-azido)-OH self-assembled into porous spherical structures, whereas the peptides H-Phe(4-azido)-Phe-OH and H-Phe-Phe (4-azido)-OH [19] was describes too. Ile-Gln-Ser-Pro-His-Phe-Phe (IQSPHFF) identified and found to undergo self-assembly into microparticles in solution [20]. Boc-Ile-Ile-OMe, Boc-Phe-Phe-Phe-Ile-Ile-OMe and Boc-Trp-Ile-Ile-OMe showed nanotubular structures [21]. Self-

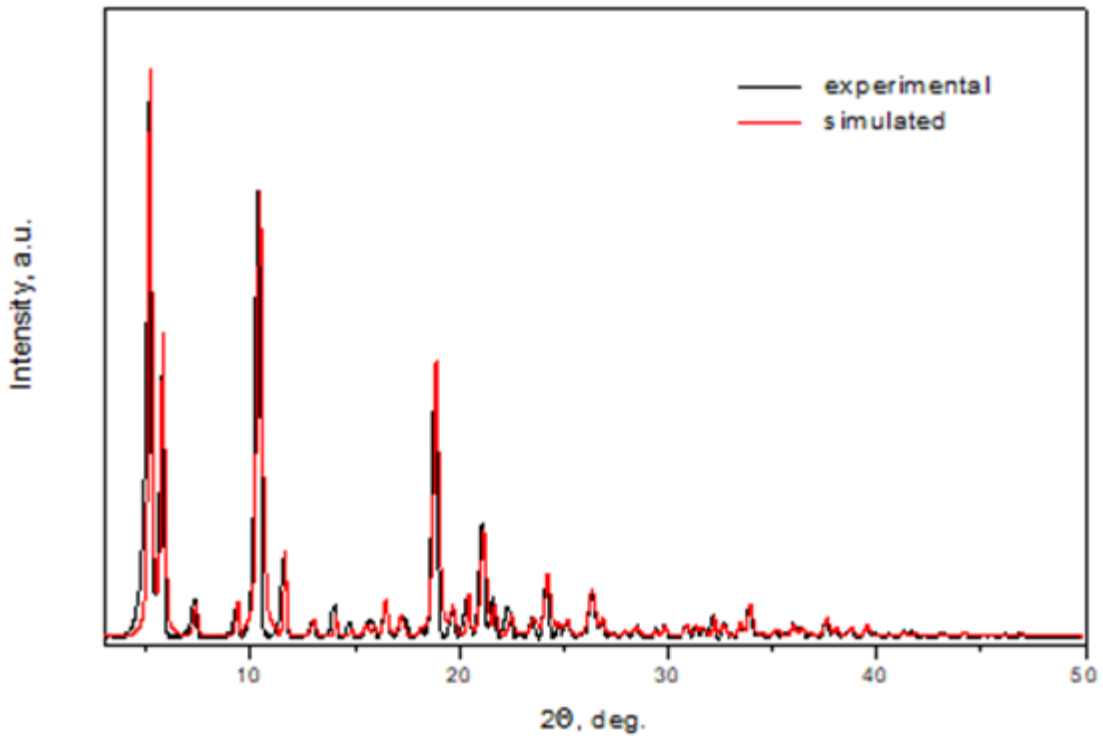

Figure 1. Experimental and simulated XRD patterns of Leucine dipeptide PNTs.

assembly of aromatic CDP (Phe-Phe) into fibre bundles with 1–2 mm thick and several millimetres long is described [22]. Using zwitterionic Phe-Phe dipeptides and straightforward experimental procedures tubular and vesicular dipeptide structures [23], oriented self-assembly dipeptides films [24] have been grown.

Piezoelectricity is the ability of no centrosymmetric crystals to produce mechanical stress/strain under electric field or charge under mechanical stress. This fundamental property has long been used in numerous devices microelectromechanical systems (MEMS): such as acoustic transducers, sensors and actuators, piezoelectric motors, rf resonators, SAW filters, micro energy generators (energy harvesting). To date, one of the most popular energy harvesting or piezoelectric sensor materials is lead zirconium titanate (PZT) because of its high piezoelectric constant and electromechanical coupling factor. However, the critical issues currently limiting its wide applications lie in its fragility and environmental hazardous element (lead). To address these problems, much effort has been expended on the piezoelectric organic compounds and their composites (PNTs) [25]. Strong piezoelectric activity in glycine and diphenylalanine nanotubes (FF PNTs) holds a great promise for using piezoeffect in such applications was discovered [26-29].

We investigated the electromechanical properties of new PNTs: Di-Leucine (LL).

Table 1. Crystal data of Leucine dipeptide.

a, Å	b, Å	c, Å	α	β	γ	V, Å^3
33.087	16.999	6.062	90°	90°	90°	3409.55

Table 2. Reflection indices, d_{hkl} values and relative peak intensities in the simulated XRD patterns for XRD of Leucine dipeptide on Fig. 1.

No.	Pos. [°2Th.]	h	k	l	d-spacing [Å]	Rel. Int. [%]
1	5.1829	2	0	0	17.05077	100
2	5.7972	1	1	0	15.24548	52.59
3	7.3749	2	1	0	11.98719	5.72
4	9.3783	3	1	0	9.43046	6.22
5	10.4337	4	0	0	8.4788	78.96
6	11.6477	2	2	0	7.59762	15.29
7	13.0209	3	2	0	6.79934	3.07
8	14.0963	5	1	0	6.28292	3.92
9	14.8404	1	0	1	5.96952	1.15
10	15.5556	2	0	1	5.69666	2.11
11	15.9248	1	3	0	5.56539	1.86
12	16.4674	2	3	0	5.38321	6.69
13	17.2118	3	1	1	5.15204	3.63
14	18.0761	1	2	1	4.90761	0.9
15	18.8833	6	2	0	4.69959	49.52
16	19.6784	5	0	1	4.51148	4.6
17	20.437	5	3	0	4.3457	7.87
18	21.1547	7	2	0	4.19985	18.99
19	21.6979	8	1	0	4.09592	5.39
20	22.4735	3	4	0	3.95629	3.69
21	22.9621	3	3	1	3.8732	0.32
22	23.5433	7	0	1	3.77889	3.08
23	24.2113	7	3	0	3.67613	11.31
24	24.7465	5	4	0	3.59782	1.93
25	25.1491	5	3	1	3.54113	2.82
26	26.3298	1	5	0	3.38495	8.62
27	26.8473	10	1	0	3.32087	3.24
28	27.2507	3	5	0	3.27262	0.63
29	27.9538	7	4	0	3.19188	0.89
30	28.4699	9	3	0	3.13518	1.73
31	29.3714	5	5	0	3.04098	0.96
32	29.8293	9	2	1	2.99533	1.89
33	30.8676	11	2	0	2.8969	2.12
34	31.362	4	0	2	2.85235	1.85
35	31.6858	7	4	1	2.82393	1.75
36	32.1921	12	1	0	2.78067	4.25
37	32.6298	11	0	1	2.74436	2.2
38	33.4582	12	2	0	2.67829	2.59
39	33.9177	2	3	2	2.64305	6.09
40	34.4937	3	3	2	2.60022	0.44
41	35.192	4	3	2	2.55021	1.21
42	35.9805	11	4	0	2.49611	2.27
43	36.4499	8	0	2	2.46504	1.39
44	36.7902	2	4	2	2.44302	0.5
45	37.5935	14	1	0	2.39264	3.48
46	38.0678	13	3	0	2.36391	1.39
47	38.7637	14	2	0	2.32306	1.54
48	39.5188	11	5	0	2.2804	1.95
49	40.5768	14	3	0	2.22335	0.31
50	41.2749	4	5	2	2.18734	1
51	41.8341	11	0	2	2.15939	0.62
52	43.0997	16	1	0	2.09887	0.46
53	44.168	7	5	2	2.05055	0.74
54	46.1086	0	2	3	1.96867	0.27
55	46.8749	3	2	3	1.93665	0.5

2. EXPERIMENTAL DETAILS

Di-peptides compounds Di-Leucine (LL) were used (Bachem, Switzerland: M-1535.0005 H-Leu-Leu-OH). PNTs were self-assembled by dissolving the dipeptide in the lyophilized form (Bachem, Switzerland) in 1,1,1,3,3,3-hexafluoro-2-propanol at a concentration of 20-100mg/ml. The stock solution was then diluted to a final concentration of 2mg/ml in doubledistilled water for the self-assembly process to occur. The diluted solution was deposited onto Pt-coated silicon substrates and left overnight for drying at room temperature.

The structural features were analyzed by X-ray diffraction (XRD) technique using a Rigaku X-ray diffractometer having a CuKα radiation source with λ = 1.541 Å.

Atomic Force Microscopy (AFM) measurements were carried out using a Veeco AFM Multimode Nanoscope (IV) MMAFM-2, Veeco microscopy. Local piezoelectric properties of the PNTs were visualized simultaneously by using Atomic Force Microscopy (AFM) in contact mode and piezoresponse force microscopy (PFM) methods [30]. The PFM technique is based on the converse piezoelectric effect, which is a linear coupling between the electrical and mechanical properties of a material. Since all ferroelectrics exhibit piezoelectricity, an electric field applied to a ferroelectric sample result in changes of its dimensions. To detect the polarization orientation the AFM tip is used as a top electrode, which is moved over the sample surface. Piezoresponse force microscopy relies on the linear strain response as a function of the external electric field. Regardless of this linear response that is inherent to materials without center of inversion symmetry, all materials dispose of a quadratic strain response in the electric field, known as electrostriction. Electrostriction therefore provides a local electromechanical response at the second harmonic of the AC voltage in piezoresponse force microscopy. This electrostrictive response provides valuable insight into the material properties in itself. It becomes particularly interesting in systems where the symmetry of the crystal does not allow for particular modes of deflection of the AFM, especially for lateral deflections. In this scenario, this type of microscopy provides a powerful imaging tool for local material defects like misfit dislocations. EFM (Electric Force Microscopy) oscillates a conducting AFM tip to sense electric force gradients. Usually, this is done in 2 passes - one to measure the topography in a standard dynamic mode and the second to "lift" a set amount above the recorded profile to measure electric field strength. Using the phase signal, a map of the gradient of the electric field is created. Kelvin Probe Force Microscopy (KFM) mode

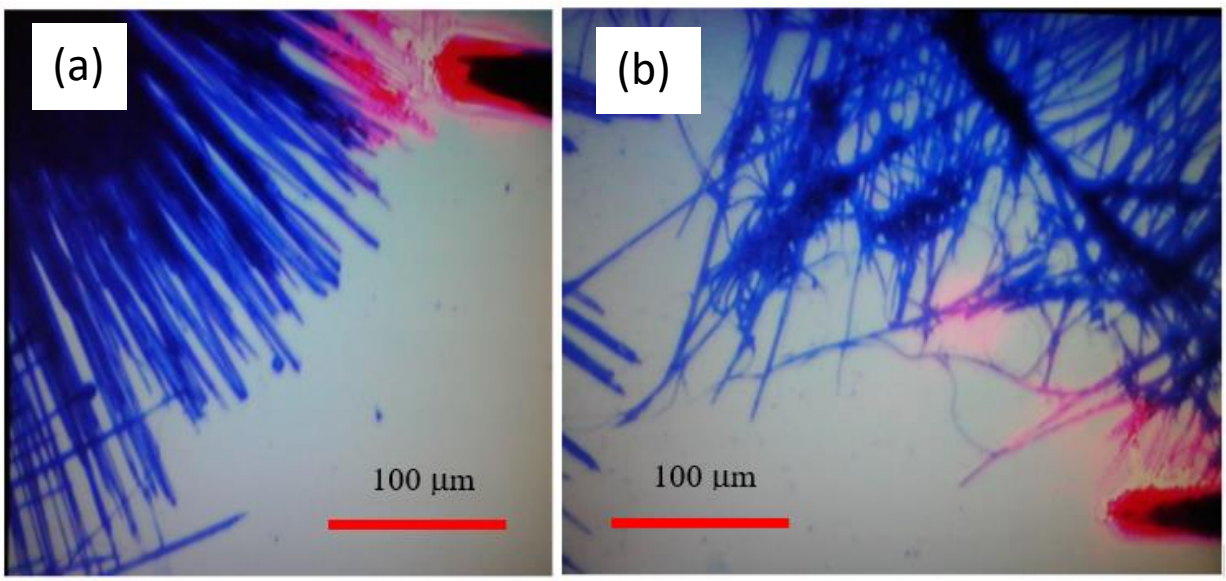

Figure 2. Optical images of LL PNTs.

measures the work function of the surface. It is also known as surface potential microscopy.

3. RESULTS AND DISCUSSION

Fig. 1 shows powder diffraction patterns of L,L-dileucine obtained in a similar way used for preparation of in this study for LL PNTs. Parameters of unit cell determined by XRD analysis (Table 1) is similar reported by C. Gorbitz [1]: a= 5.3524 Å, b= 16.7600 Å, c= 33.312 Å, V= 2988.3 Å^3. Rietveld-refined X-ray diffraction pattern of the dipeptide L,L-dileucine analysis was done using space group $P2_12_12_1$ (Table 1, Fig.1). Strong difference in unit cell volume (14%) and parameter a (12%) can be explain by presents of water in the structure.

Figures 2 show representative optical microscopy images of the investigated LL PNTs samples. As expected, as-grown PNTs demonstrate a variety of tubes of different lengths and diameters due to their spontaneous self-assembly on the substrate surface.

The cross section of the in-plane PFM (Figure 3c) shows the piezoelectric profile has a decrease in signal at the centre of the tube. It can be assumed that such a profile is typical for tubes with a large ratio of outer to inner diameter, where the internal cavity (in the centre of the section) has a significantly smaller effective thickness and the resulting signal is less than on the wall).

It is well known that the magnitude of the piezoresponce signal in PFM depends on measurement geometry and orientation. The figure 4 shows that with an arbitrary distribution of tubes on the surface of the substrate, the recorded signal changes both in magnitude and sign. In-plane (IP) PFM image of peptide nanotubes with rotation demonstrating apparent contrast reversal. Blue

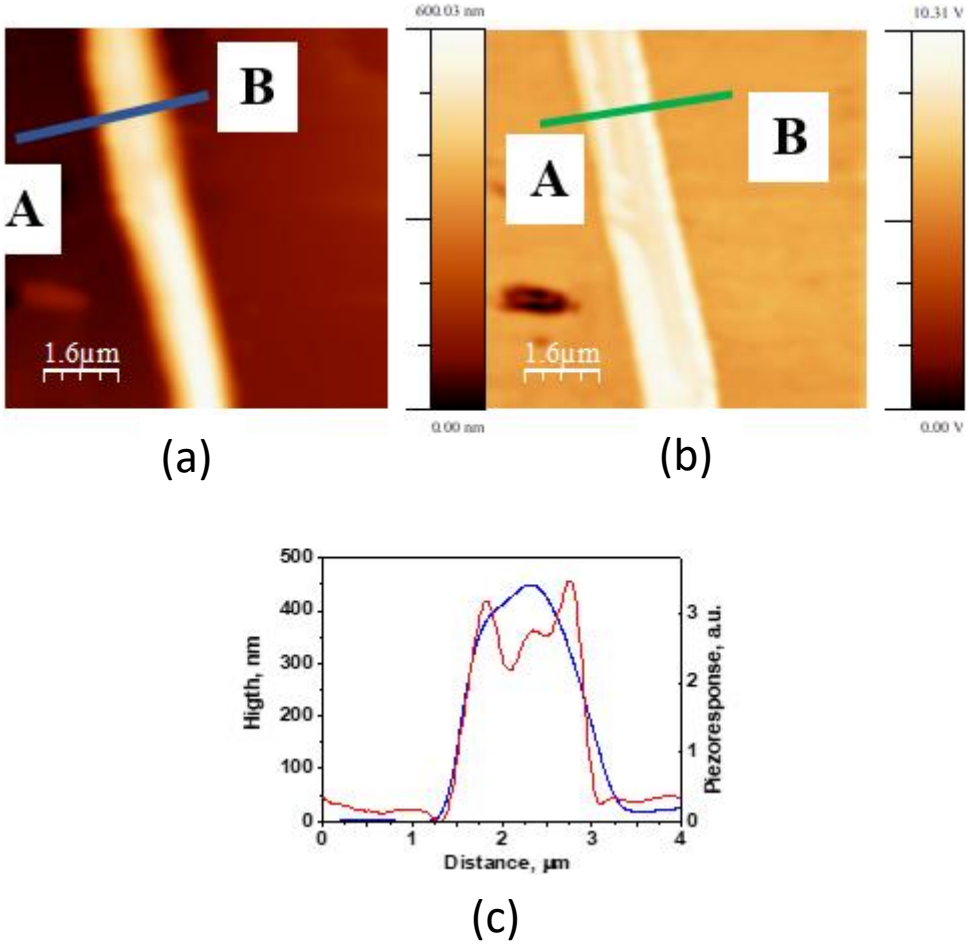

Figure 3. LL PNTs. (a) Topography image. (b) In plane PFM image. Cross sections of AB - (c).

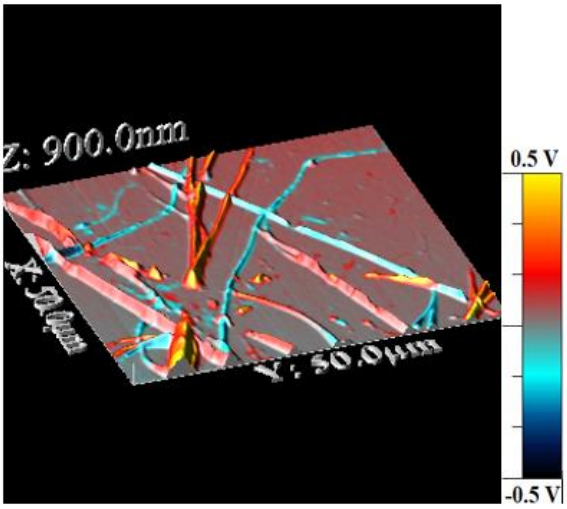

Figure 4. 3D LL PNTs topography and in-plane PFM (color) image.

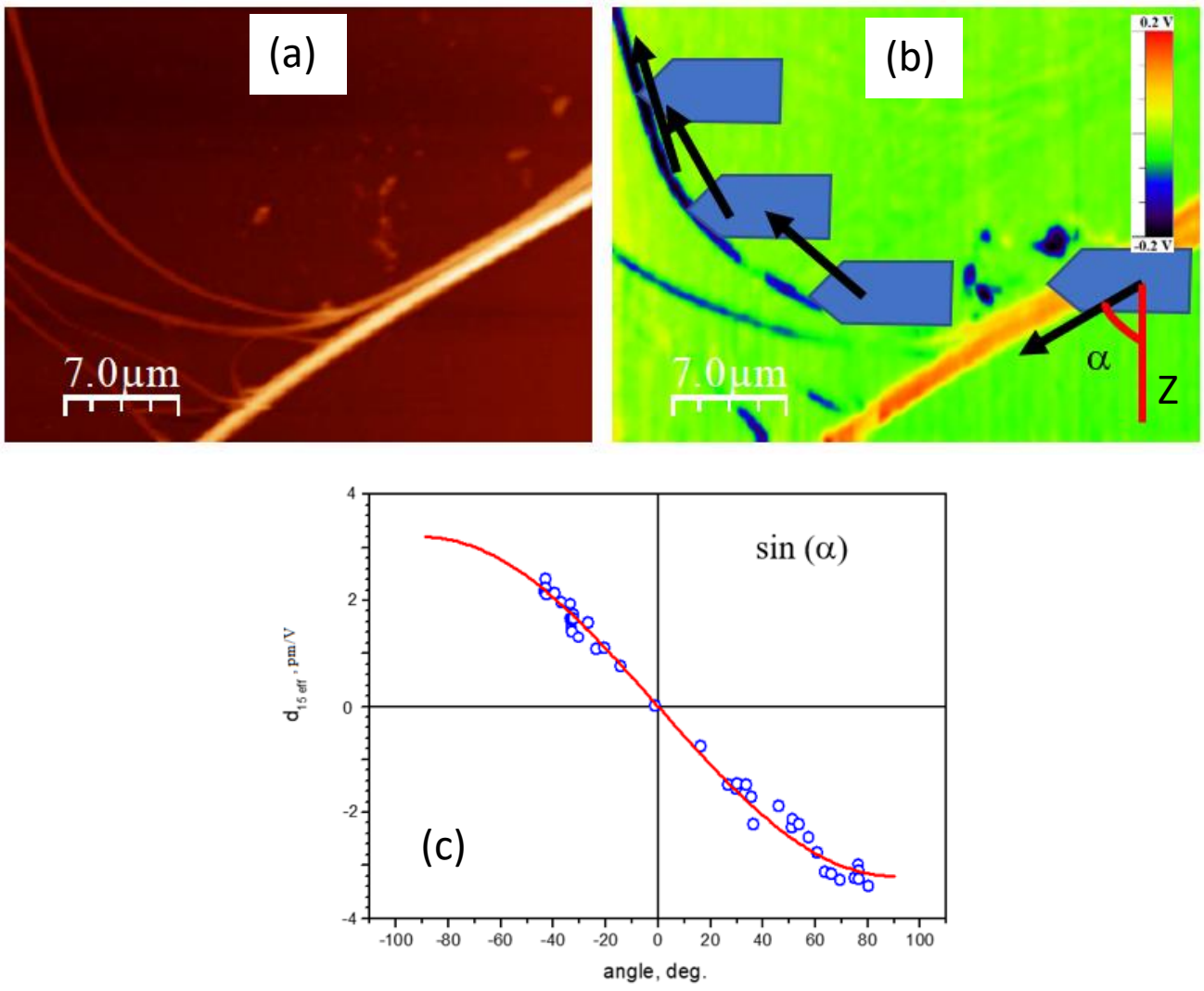

Figure 5. LL PNTs. (a) Topography and (b) PFM image. (c) IP signal angle dependences for representative tube.

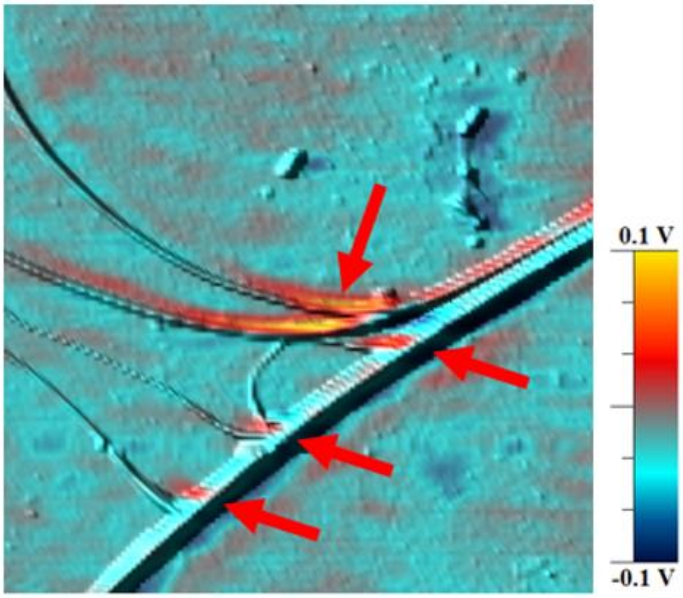

Figure 6. 3D LL PNTs. (a) Topography and KFM (color) image.

polarization orientations of the tubes.

For the arbitrary orientation of the crystal, possible to use equation, $d_{15}V_{ac}$ sinα (Fig. 5b), applies, where now angle is the angle between the scanning direction and the Z-axis. As shown in Figure 3d, we observed this dependence with the maximum value of 3.2 pm/V (Fig.5c).

Piezoelectric polarization leads to charge localization in the same way. For such a highly asymmetric case as tubes, when the polarization is directed along, one can expect an accumulation of charges at the ends of the tubes. In the case of a more significant reorientation of polarization, in the case of merging of two tubes, localization of charges can also be assumed. The method Kelvin Probe Force Microscopy (KFM) was used to study the charge distribution (Fig.6). It can be seen that at the points of contact of the nanotubes there is an increased contrast (indicated by arrows), which corresponds to the localization of the charges.

4. CONCLUSIONS

Experimental local measurements of the parameters of the piezo response of LL tubes and LL microcrystals were carried out. A study of the angular dependence of the orientation of the tubes showed agreement with the geometric measurement model. The effect of tube curvature on the electromechanical and electrostatic characteristics of the tubes was studied. The data obtained showed that LL-PNTs may be of the most promising interest for further use as stronger ferroelectric compounds.

ACKNOWLEDGMENTS

This work was developed in the scope of the Project “Agenda ILLIANCE” [C644919832-00000035 | Project no. 46], financed by PRR – Recovery and Resilience Plan under the Next Generation EU from the European Union. This work also was supported, in terms of TEMA Research Infrastructure equipment, by the projects UIDB/00481/2020 and UIDP/00481/2020 - Fundação para a Ciência e a Tecnologia; and CENTRO-01-0145-FEDER-022083 - Centro Portugal Regional Operational Programme (Centro2020), under the PORTUGAL 2020 Partnership Agreement, through the European Regional Development Fund.

REFERENCES

1. C. H. Gorbitz, Nanotube Formation by Hydrophobic Dipeptides, *Chem Eur J.*, **7**, 5153–5159 (2001).
2. E. Gazit, A possible role for π-stacking in the self-assembly of amyloid fibrils, *FASEB J.*, **16**, 77-83 (2002).
3. Silvia Marchesan, Attilio V. Vargiu and Katie E. Styan, The Phe-Phe Motif for Peptide Self-Assembly in Nanomedicine, *Molecules* **20**, 19775–19788 (2015).

4. Yingying Ding, Ding Li, Bin Li, Kai Zhao, Wei Du, Jinyun Zheng, Minghui Yang, A water-dispersible, ferrocene-tagged peptide nanowire for amplified electrochemical immunosensing, *Biosensors and Bioelectronics* **48** 281–286 (2013).
5. Ehud Gazit, Reductionist Approach in Peptide-Based Nanotechnology, *Annu. Rev. Biochem.* **87**, 533–53 (2018).
6. Sayanti Brahmachari, Zohar A. Arnon, Anat Frydman-Marom, Ehud Gazit, and Lihi Adler-Abramovich, Diphenylalanine as a Reductionist Model for the Mechanistic Characterization of β-Amyloid Modulators, *ACS Nano* **11**, 5960−5969 (2017).
7. R. C. Naber, K. Asadi, P. W. Blom, D. M. de Leeuw, and B. de Boer, Organic Nonvolatile Memory Devices on Ferroelectricity, *Adv. Mater.* **22**, 933 (2010).
8. S. H. Sung and B. W. Boudouris, Systematic Control of the Nanostructure of Semiconducting-Ferroelectric Polymer Composites in Thin Film Memory Devices, *ACS Macro Lett.* **4**, 293 (2015).
9. Zohar A. Arnon, Dorothea Pinotsi, Matthias Schmidt, Sharon Gilead, Tom Guterman, Aditya Sadhanala, Shahab Ahmad, Aviad Levin, Paul Walther, Clemens F. Kaminski, Marcus Fändrich, Gabriele S. Kaminski Schierle, Lihi Adler-Abramovich, Linda J. W. Shimon, and Ehud Gazit, Opal-like Multicolor Appearance of Self-Assembled Photonic Array, *ACS Appl. Mater. Interfaces* **10**, 20783−20789 (2018).
10. Wei-Hsien Hsieh, Jiahorng Liaw, Applications of cyclic peptide nanotubes (cPNTs), *Journal of food and drug analysis* **27**, 32-47 (2019).
11. Lihi Adler-Abramovich and Ehud Gazit, The physical properties of supramolecular peptide assemblies: from building block association to technological applications, *Chem. Soc. Rev.* **43**, 6881 (2014).
12. Michal Pellach, Sudipta Mondal, Linda J. W. Shimon, Lihi Adler-Abramovich, Ludmila Buzhansky, and Ehud Gazit, Molecular Engineering of Self-Assembling Diphenylalanine Analogues Results in the Formation of Distinctive Microstructures, *Chem. Mater.* **28**, 4341−4348 (2016).
13. Samaneh Beheshti, Sanela Martic, and Heinz-Bernhard Kraatz, Hierarchical Organization of Ferrocene–Peptides, *Chem. Eur. J.* **18**, 9099 – 9105 (2012).
14. Meital Reches and Ehud Gazit, Designed aromatic homo-dipeptides: formation of ordered nanostructures and potential nanotechnological applications, *Phys. Biol.* **3**, S10–S19 (2006).
15. Surajit Ghosh, Lihi Adler-Abramovich, Ehud Gazit, Sandeep Verma, Spacer driven morphological twist in Phe-Phe dipeptide conjugates, *Tetrahedron* **69**, 2004-2009 (2013).
16. Jianxiu Wang, Ding Li, Minghui Yang and Yi Zhang, A novel ferrocene-tagged peptide nanowire for enhanced electrochemical glucose biosensing, *Anal. Methods* **6**, 7161 (2014).
17. Magdalena Jaworska, Agata Jeziorna, Ewelina Drabik, and Marek J. Potrzebowski, Solid State NMR Study of Thermal Processes in Nanoassemblies Formed by Dipeptides, *J. Phys. Chem. C* 116, 12330−12338 (2012).
18. Gagandeep Kaur, Lihi A. Abramovich, Ehud Gazit and Sandeep Verma, Ultrastructure of metallopeptide-based soft spherical morphologies, *RSC Adv.* **4**, 64457–64465 (2014).
19. Sivan Yuran, Yair Razvag, Priyadip Das and Meital Reches, Self-assembly of azide containing dipeptides, *J. Pept. Sci.* **20**, 479–486 (2014).
20. Ran Wei, Cheng-Cheng Jin, Jing Quan, Hua-li Nie, Li-Min Zhu, A Novel Self-Assembling Peptide with UV-Responsive Properties, *Biopolymers* 101, 272-278 (2013).
21. Chilukuri Subbalakshmi, Sunkara V. Manoram and Ramakrishnan Nagaraj, Self-assembly of short peptides composed of only aliphatic amino acids and a combination of aromatic and aliphatic amino acids, *J. Pept. Sci.* **18**, 283–292 (2012).
22. T. Govindaraju, Spontaneous self-assembly of aromatic cyclic dipeptide into fibre bundles with high thermal stability and propensity for gelation, *Supramolecular Chemistry* **23**, 759–767 (2011).
23. Gokhan Demirel, Niranjan Malvadkar, and Melik C. Demirel, Control of Protein Adsorption onto Core-Shell Tubular and Vesicular, Structures of Diphenylalanine/Parylene, *Langmuir* **26(3)**, 1460–1463 (2010).
24. Gokhan Demirel, and Fatih Buyukserin, Surface-Induced Self-Assembly of Dipeptides onto Nanotextured Surfaces, *Langmuir* **27**, 12533–12538 (2011).
25. Balakrishnan Karthikeyan, Aswini Kumar Giri, Victor J. Hruby, Entrap and release of Phe–Phe nanotubes in sol–gel derived silicate matrix: study through nanosilver interaction, *J Sol-Gel Sci Technol* **72**, 534–542 (2014).
26. Andrei Kholkin, Nadav Amdursky, Igor Bdikin, Ehud Gazit, Gil Rosenman, Strong piezoelectricity in bioinspired peptide nanotubes, *ACS Nano* **4 (2)**, 610–614 (2010).
27. Igor Bdikin, Vladimir Bystrov, Svitlana Kopyl, Rui P. G. Lopes, Ivonne Delgadillo, José´ Gracio, Elena Mishina, Alexander Sigov, and Andrei L. Kholkin, Evidence of ferroelectricity and phase transition in pressed diphenylalanine peptide nanotubes, *Appl. Phys. Let.* **100**, 043702 (2012).
28. Igor Bdikin, Vladimir Bystrov, Ivonne Delgadillo, José Gracio, Svitlana Kopyl, Maciej Wojtas, Elena Mishina, Alexander Sigov, and Andrei L. Kholkin, Polarization switching and patterning in self-assembled peptide tubular structures, *J. Appl. Phys.* **111**, 074104 (7p) (2012).
29. S. Safaryan, V. Slabov, S. Kopyl, K. Romanyuk, I. Bdikin, S. Vasilev,P. Zelenovskiy, V. Shur, E. Uslamin, E. Pidko, A. Vinogradov,A. Kholkin, Diphenylalanine-Based Microribbons for Piezoelectric Applications via Inkjet Printing, *ACS Applied Materials & Interfaces* **10**, 12, 10543-10551 (2018).
30. A. Roelofs, T. Schneller, K Szot, and R Waser, Piezoresponse force microscopy of lead titanate nanograins possibly reaching the limit of ferroelectricity, *Applied Physics Letters* **81 (27)**, 5231-5233) (2002).